

An Introduction to Analytic Models of Halo Formation

Andrew R. Zentner

Kavli Institute for Cosmological Physics &
Department of Astronomy and Astrophysics
The University of Chicago
Chicago, IL 60637, USA

1 Introduction

In this lecture, I review the standard excursion set (also called extended Press-Schechter) approach to halo formation. I begin with some preliminaries that serve to define my notation and several common conventions in § 2. I review the heuristic argument of Press & Schechter (1974) used to derive their analytic mass function in § 3. In this section I also draw attention to the most obvious weakness of the Press & Schechter (1974) argument, often referred to as the cloud-in-cloud problem. In § 4 I review the way in which the cloud-in-cloud problem is solved using the theory of excursion sets of the density field.

The excursion set approach is very powerful and yields a great deal of insight into halo formation and halo clustering. One of the most immediate applications of the excursion set approach is to predict the clustering properties of dark matter halos relative to the dark matter. I review the issue of halo bias in the context of the excursion set theory in § 5. The bias relation derived in § 5 was derived prior to widespread use of excursion set theory, but this section serves partially as a warm-up for the more complex arguments that follow. In § 6, I review excursion set predictions for halo conditional mass functions, halo accretion rates, and halo formation times. The culmination of this review is the algorithm for generating Monte Carlo merger histories on a halo-by-halo basis using the excursion set theory and this is the subject of § 7.

Recent advancement in both theoretical methods and observational data have emphasized the weakness of the simplest implementation of the excursion set model. Nevertheless, the basic idea of the excursion set model is extremely valuable because it provides a toolbox for making quick estimates and remains one of the principle frameworks for qualitative reasoning and understanding of complex processes. I address briefly extensions of the excursion set models and proposed improvements in the final section of this review, § 8. The reference list contained in these notes is by no means an exhaustive review of the literature on analytic halo formation or the excursion set approach and many important contributions have been omitted in the interest of brevity. However, the references should be sufficient to develop the fundamental logic of the excursion set approach.

2 Notation and Conventions

In the following, I consider fluctuations in the density field $\rho(\vec{x})$ described by the density contrast $\delta(\vec{x}) \equiv [\rho(\vec{x}) - \rho_M]/\rho_M$, where ρ_M is the mean mass density in the universe and \vec{x} is a comoving coordinate. In the standard paradigm, the universe is endowed with primordial density fluctuations during an epoch of cosmological inflation and the primordial density contrast is a statistically homogeneous and isotropic Gaussian random field.

The Fourier transform of the density contrast is given by the convention

$$\delta(\vec{k}) = \int d^3x \delta(\vec{x}) e^{i\vec{k}\cdot\vec{x}} \quad (1)$$

with the inverse transform

$$\delta(\vec{x}) = \frac{1}{(2\pi)^3} \int d^3k \delta(\vec{k}) e^{-i\vec{k}\cdot\vec{x}}. \quad (2)$$

Notice that the $\delta(\vec{k})$ have dimensions of volume and that for a real-valued field $\delta(\vec{x})$, the Fourier coefficients obey the relation $\delta(-\vec{k}) = \delta^*(\vec{k})$. We have implicitly assumed that there is some very large cut-off scale $L \equiv V^{1/3}$ that renders the integral $\int |\delta(\vec{x})| d^3x$ finite and that this scale is much larger than any other scale of interest so that it plays no meaningful role. Using these conventions, one can compute the two-point function $\xi(\vec{r}) \equiv \langle \delta(\vec{x}) \delta(\vec{x} + \vec{r}) \rangle$ in terms of the Fourier coefficients, where the average is taken over all space. The two-point function is a function only of the amplitude of \vec{r} due to isotropy, and

the result is

$$\xi(r) = \frac{1}{2\pi^2} \int k^3 V^{-1} |\delta(k)|^2 \frac{\sin(kr)}{kr} d \ln k. \quad (3)$$

The correlation function is the Fourier transform of the power spectrum

$$P(k) \equiv V^{-1} \langle |\delta(k)|^2 \rangle, \quad (4)$$

where the average is over an ensemble of universes with the same statistical properties. The power spectrum has dimensions of volume and so a more easily-interpreted quantity is the dimensionless combination

$$\Delta^2(k) \equiv k^3 P(k) / 2\pi^2. \quad (5)$$

The correlation function $\langle \delta^2 \vec{x} \rangle$ is simply the mass variance. From Eq. (3), $\Delta^2(k)$ is the contribution to the mass variance from modes in a logarithmic interval in wavenumber, so that $\Delta^2(k) \sim 1$ indicates order unity fluctuations in density on scales of order $\sim k$.

In the standard, cold dark matter (CDM) model, $\Delta^2(k)$ increases with wavenumber (at least until some small scale determined by the physics of the production of the CDM in the early universe), but we observe the density field smoothed with some resolution. Therefore, a quantity of physical interest is the density field smoothed on a particular scale R_W ,

$$\delta(\vec{x}; R_W) \equiv \int d^3 x' W(|\vec{x}' - \vec{x}|; R_W) \delta(\vec{x}') \quad (6)$$

The function $W(x; R_W)$ is the window function that weights the density field in a manner that is relevant for the particular application. According to the convention used in Eq. (6), the window function (sometimes called *filter* function) has units of inverse volume by dimensional arguments. It is also useful to think of a window as having a particular window volume V_W . The window volume can be obtained operationally by normalizing $W(x)$ such that it has a maximum value of unity and is dimensionless. Call this new dimensionless window function $W'(x)$. The volume is given by integrating to give $V_W = \int d^3 x W'(x)$. In this way, one thinks of the window weighting points in the volume. It should be clear that $W(x) = W'(x) / V_W$. Roughly speaking, the smoothed field is the average of the density fluctuation in a region of volume $V_W \sim R_W^3$. The Fourier transform of the smoothed field is

$$\delta(\vec{k}; R_W) \equiv W(\vec{k}; R_W) \delta(\vec{k}), \quad (7)$$

where $W(\vec{k}; R_W)$ is the Fourier transform of the window function.

The most natural choice of window function is simply a sphere in real space so that

$$W(x; R_W) = \begin{cases} \frac{3}{4\pi R_W^3} & (x \leq R_W) \\ 0 & (x > R_W) \end{cases}. \quad (8)$$

In this case, the smoothed field is the average density in spheres of radius R_W about point \vec{x} . The window volume is simply $V_W = 4\pi R_W^3/3$. However, this choice of window has the undesirable property that the sharp transition in configuration space leads to power on all scales in Fourier space. Therefore, it is often convenient to smooth the boundary in real space. Moreover, as I discuss below, it is often convenient to introduce particular window functions to ensure that the smoothed field has particular properties. The three most commonly used window functions are the real-space tophat window of Eq. (8), with Fourier transform

$$W(k; R_W) = \frac{3[\sin(kR) - kR \cos(kR)]}{(kR)^3}, \quad (9)$$

the Fourier-space tophat window, and the Gaussian window. The Fourier-space tophat is defined in Fourier space as

$$W(k; R_W) = \begin{cases} 1 & (k \leq R_W^{-1}) \\ 0 & (k > R_W^{-1}) \end{cases}, \quad (10)$$

and is

$$W(x; R_W) = \frac{1}{2\pi^2 R_W^3} \frac{(\sin(xR_W^{-1}) - xR_W^{-1} \cos(x/R_W^{-1}))}{(xR_W^{-1})^3} \quad (11)$$

in real space. A disadvantage of this window is that it does not have a well-defined volume. This concern creeps up repeatedly in what follows. The Gaussian window is

$$W(x; R_W) = \frac{\exp(-x^2/2R_W^2)}{(2\pi)^{3/2} R_W^3} \quad (12)$$

with a Fourier transform that also has the form of a Gaussian

$$W(k; R_W) = \exp(-k^2/2R_W^{-2}). \quad (13)$$

The volume of the Gaussian window is $V_W = (2\pi)^{3/2} R_W^3$.

The density fluctuation field is assumed to be a Gaussian random variable so the smoothed density fluctuation field $\delta(\vec{x}; R)$ is then a Gaussian random variable as well because represents a sum of Gaussians. The variance of $\delta(\vec{x}; R)$ can be computed just as before [Eq. (3)] and is

$$\sigma^2(R) = \langle \delta^2(\vec{x}; R) \rangle = \int d \ln k \Delta^2(k) |W(k; R)|^2. \quad (14)$$

Thus, the probability of attaining a value of $\delta(\vec{x}; R)$ between δ and $\delta + d\delta$ is

$$P(\delta; R)d\delta = \frac{1}{\sqrt{2\pi\sigma^2(R)}} \exp[-\delta^2/2\sigma^2(R)]d\delta. \quad (15)$$

It is common to refer to the smoothing scale as either a length, as above, or a mass given by the mean density multiplied by the volume of the window $M = \rho_M V_W$. The left panel of Fig. 1 depicts a standard model power spectrum expressed as the variance of the smoothed density field, smoothed with a real-space tophat and shows the smoothing scale in terms of both mass and length. The right panel of Fig. 1 shows the *rms* density fluctuation per logarithmic interval in wavenumber $\Delta(k)$. The power spectra were computed assuming $\Omega_M = 1 - \Omega_\Lambda = 0.3$, $h = 0.7$, $\sigma_8 = 0.93$, and $\Omega_B h^2 = 0.022$.

3 The Press-Schechter Mass Function

Press & Schechter (1974) derived a relation for the mass spectrum of virialized objects from the hierarchical density field. In hierarchical models, there is structure on all scales so that the variance $\sigma^2(R) \rightarrow \infty$ as the smoothing scale $R \rightarrow 0$. Press & Schechter (1974) essentially assumed that objects will collapse on some small scale but that the nonlinearities introduced by these virialized objects do not affect the collapse of overdense regions on much larger scales. Strictly speaking, this is not correct; however, it is approximately true when primordial power spectra are such that the additional large-scale power generated by nonlinearities is small compared to the primordial fluctuations on these scales. Moreover, this assumption leads to a simple parsing of the ingredients in the formation of nonlinear structure. The first ingredient is the statistics of the initial spectrum of density fluctuations. In the standard picture this is set during the inflationary epoch. The second ingredient is the evolution of overdensities according to linear perturbation theory. This is encapsulated in the growth function $D(a) = \delta(k, a)/\delta(k, a = 1)$ which is

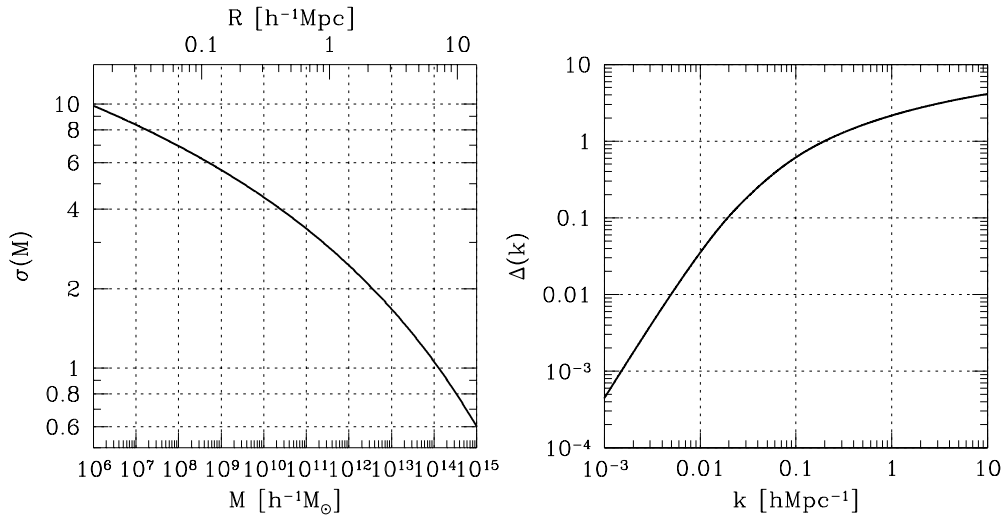


Figure 1: Power spectra in the standard Λ CDM cosmology with $\Omega_M = 1 - \Omega_\Lambda = 0.3$, $h = 0.7$, $\sigma_8 = 0.93$, and $\Omega_B h^2 = 0.022$. The left panel shows the mass variance smoothed with a real space tophat window as a function of the smoothing mass or smoothing radius [Eq. (14)]. The right panel shows the rms density fluctuation per logarithmic interval of wavenumber as a function of wavenumber [Eq. (3)].

specified by the evolution of the background cosmology (*e.g.*, Carroll et al., 1992; Bildhauer et al., 1992; Lacey & Cole, 1993). The last ingredient is the threshold for collapse is determined by examining the nonlinear collapse of spherical overdensities.

Press & Schechter (1974) stated that the likelihood for collapse of objects of a specific size or mass ($R \propto M^{1/3}$) could be computed by examining the density fluctuations on the desired scale. They continued by using a model for the collapse of a spherical tophat overdensity to argue that collapse on scale R should occur roughly when the smoothed density on that scale exceeds some threshold.

The implementation of the Press & Schechter (1974) prescription is simple. The mass within a region in which the smoothed density fluctuation (dictated by the linear theory) is the critical value δ_c , at some redshift z , corresponds to an object that has just virialized with mass $M(R)$. The relationship between mass and smoothing scale is set by the volume of the window function. As an example, the relationship is $M = 4\pi\rho_M R^3/3$ for a tophat window and $M = (2\pi)^{3/2}\rho_M R^3$ for a Gaussian window. Further, any region that exceeds the critical density fluctuation threshold, will meet that threshold when smoothed on some larger scale $R' > R$. Consequently, the cumulative probability for a region to have a smoothed density above threshold gives the fractional volume occupied by virialized objects larger than the smoothing scale $F(M)$. Integrating Eq. (15), this probability is

$$F(M) = \int_{\delta_c}^{\infty} P(\delta; R) d\delta = \frac{1}{2} \operatorname{erfc}\left(\frac{\nu}{\sqrt{2}}\right), \quad (16)$$

where $\operatorname{erfc}(x)$ is the complementary error function, and $\nu \equiv \delta_c/\sigma(M)$ is the height of the threshold in units of the standard deviation of the smoothed density distribution. In this model, collapse of mass M is defined so that it occurs when the smoothed density fluctuation is δ_c on the appropriate scale. Thus there is a typical scale that is collapsing at the present epoch, M_* , when the variance is $\sigma(M_*) = \delta_c$.

In the hierarchical power spectra that we consider, $\sigma(R)$ becomes arbitrarily large as R becomes arbitrarily small. Thus, $F(0)$ in Eq. (16) should give the fraction of all mass in virialized objects; however, $\operatorname{erfc}(0) = 1$ so that Eq. (16) states that only half of the mass density of the universe is contained in virialized objects. Press & Schechter (1974) noted this as a problem associated with not counting underdense regions in the integral Eq. (16). They

argued that underdense regions will collapse onto overdense regions and multiplied $F(M)$ in Eq. (16) by a factor of two in order to account for all mass.

Proceeding with this extra factor of two, the number of virialized objects with masses between M and $M + dM$ is

$$\frac{dn}{dM} dM = \frac{\rho_M}{M} \left| \frac{dF(M)}{dM} \right| dM. \quad (17)$$

In terms of the mass variance, this is

$$\begin{aligned} \frac{dn}{dM} dM &= \sqrt{\frac{2}{\pi}} \frac{\rho_M}{M^2} \frac{\delta_c}{\sigma} \left| \frac{d \ln \sigma}{d \ln M} \right| \exp \left(-\frac{\delta_c^2}{2\sigma^2} \right) dM \\ &= \sqrt{\frac{2}{\pi}} \frac{\rho_M}{M^2} \nu \frac{d \ln \nu}{d \ln M} \exp \left(-\frac{\nu^2}{2} \right) dM. \end{aligned} \quad (18)$$

Without regard to the details of the shape of the power spectrum, $\sigma(M)$ or $\nu(M)$, the mass function is close to a power law $dn/dM \propto M^{-2}$ for $M \ll M_*$ and is exponentially cut-off for $M \gtrsim M_*$.

4 Excursion Set Theory of the Mass Function

A weakness of the Press & Schechter (1974) approach is that it does not account for the fact that at a particular smoothing scale $\delta(\vec{x}; R)$ may be less than δ_c , yet it may be larger than δ_c at some *larger* smoothing scale $R' > R$. It seems natural that this larger volume should collapse to form a virialized object. Clearly, the sense of including this effect is to increase the fraction of mass in collapsed objects and mitigate the factor of two discrepancy in the Press & Schechter (1974) formulas. In the literature, the issue of regions below threshold on a particular scale, but above threshold on a larger scale is referred to as the “cloud-in-cloud” problem.

To solve the cloud-in-cloud problem, it is necessary to compute the *largest* value of the smoothing scale for which the density threshold is exceeded. This was done in a formal way by Bond et al. (1991, see also Epstein 1983, Peacock & Heavens 1990, and Bower 1991) and I follow their approach quite closely. The development of Bond et al. (1991) in turn follows the elegant review of stochastic processes of Chandrasekhar (1943).

Consider again evaluating the field $\delta(\vec{x}; R)$ at various values of the smoothing scale R , at a single point \vec{x} . For now, I will suppress the argument \vec{x} and

consider $\delta(R)$ as a function of smoothing scale at a single point in space. For very large R , $\sigma(R) \ll \delta_c$ so the probability that the region lies above the boundary δ_c is vanishingly small. With decreasing R , the standard deviation becomes larger and $\delta(R)$ will eventually reach δ_c at the first up-crossing of the boundary. The problem is to compute the probability that the first up-crossing of the barrier at δ_c occurs on a scale R . For simplicity in what follows, let $S \equiv \sigma^2(R)$ and let the value of S serve to denote the smoothing scale by exploiting the fact that S is a monotonically decreasing function of R . I will then refer to the density contrast on that scale as $\delta(S)$.

Consider starting at a large smoothing scale, or small $S = S_1$, where $\delta(S_1) \equiv \delta_1 < \delta_c$. For a given change in the filtering scale ΔS , there is some distribution for the probability of reaching δ_2 after an increment $\Delta S = S_2 - S_1 > 0$. In general, this probability distribution may depend not only on the size of the step ΔS , but the field at the starting point. In this case, solving for the probability distribution of δ at a given S is nontrivial. An important special case is when the smoothing window used to define $\delta(S)$ is a k-space tophat as in Eqs. (10)-(11). In that case, increasing the filter scale corresponds to adding a set of independent modes to the smoothed density. In this special case, the transition probability for a change in density $\Delta\delta$ associated with a change in filtering scale ΔS is Gaussian with zero mean variance $S_2 - S_1 = \Delta S$, independent of the starting point.

Following Bond et al. (1991), it is common to refer to a sequence of $\delta(S_i)$ given by many subsequent increases of the smoothing scale by increments ΔS_i as a trajectory for $\delta(S)$. In the case of k-space tophat filtering of the density field, each trajectory of $\delta(S)$ executes a Brownian random walk. Three examples of such uncorrelated random walks are shown in Fig. 2. Notice that trajectories pierce the ‘‘barrier’’ at δ_c many times and drop below δ_c between subsequent up-crossings. The aim of the excursion set approach is to solve the cloud-in-cloud problem by determining the largest smoothing scale R or M , or equivalently the smallest value of the variance S , for a trajectory penetrates the barrier at δ_c .

In the case of k-space tophat filtering, the probability of a transition from δ_1 to $\delta_2 = \delta_1 + \Delta\delta$ is

$$\Pi(\delta_2, S_2) d\delta_2 = \Psi(\Delta\delta; \Delta S) d(\Delta\delta), \quad (19)$$

where

$$\Psi(\Delta\delta; \Delta S) d(\Delta\delta) = \frac{1}{\sqrt{2\pi\Delta S}} \exp\left(-\frac{(\Delta\delta)^2}{2(\Delta S)^2}\right) d(\Delta\delta) \quad (20)$$

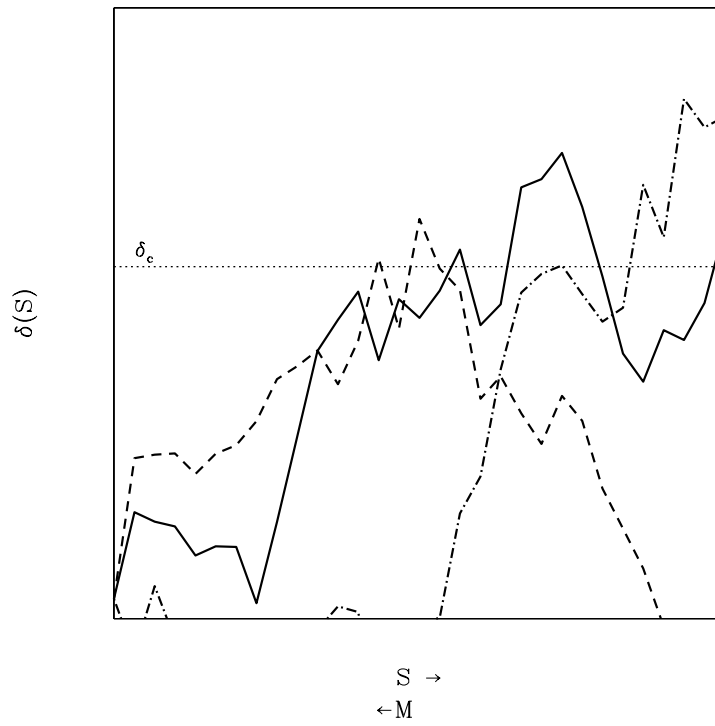


Figure 2: Three examples of random walks of $\delta(S)$ assuming each s step is independent as in the case of a sharp k -space window function. The axes are arbitrary. The horizontal dotted line represents some threshold value δ_c . Notice that trajectories may penetrate the “barrier” at δ_c many times.

is the Gaussian transition probability. Taking $S_1 = 0$, S_2 the smoothing scale of interest, and finding the probability of $\delta_2 \geq \delta_c$ returns the Press & Schechter (1974) probability for being in a collapsed object. The fact that some regions will exceed δ_c for a smaller change in S and then fall below δ_c by ΔS has not yet been accounted for.

Consider now, relating the distribution of δ at one value of the smoothing scale $\Pi(\delta, S)$ to the distribution on a subsequent step $\Pi(\delta, S + \Delta S)$ (smaller smoothing scale, larger S). This is

$$\Pi(\delta, S + \Delta S) = \int d(\Delta\delta) \Psi(\Delta\delta; \Delta S) \Pi(\delta - \Delta\delta, S). \quad (21)$$

Taylor expanding Eq. (21) for small transitions, keeping terms up to $(\Delta\delta^2)$, and integrating each term yields

$$\frac{\partial\Pi}{\partial S} = \lim_{\Delta S \rightarrow 0} \left(\frac{\langle(\Delta\delta)^2\rangle}{2\Delta S} \frac{\partial^2\Pi}{\partial\delta^2} - \frac{\langle\Delta\delta\rangle}{\Delta S} \frac{\partial\Pi}{\partial\delta} \right). \quad (22)$$

Using the fact that the transition probability is a Gaussian with $\langle\Delta\delta\rangle = 0$ and $\langle(\Delta\delta^2)\rangle = \Delta S$ reveals

$$\frac{\partial\Pi}{\partial S} = \frac{1}{2} \frac{\partial^2\Pi}{\partial\delta^2} \quad (23)$$

as the relation governing the evolution of the probability distribution Π with smoothing scale. The probability distribution Π for trajectories $\delta(S)$ that never exceed δ_c prior to some specific value of S can be obtained by solving Eq. (23) with the appropriate boundary conditions. The first boundary condition is that $\Pi(\delta, S)$ is finite as $\delta \rightarrow -\infty$. Imagining each trajectory as absorbed and removed from the sample of trajectories at the moment it first crosses the threshold at δ_c , then $\Pi(\delta_c, S) = 0$ provides the second boundary condition.

Eq. (23) may have a familiar form as it is also an equation describing diffusion with no drift or a one-dimensional heat equation describing heat flow in a long, thin, semi-infinite bar. The boundary condition at $\delta = \delta_c$ is analogous to fixing the temperature to zero at this end of the bar. Take $\delta(S_0) = \delta_0$ as an arbitrary starting point for the random walk trajectories so that the initial condition is $\Pi(\delta_0, S_0) = \delta_D(\delta_0)$ where $\delta_D(x)$ is the Dirac delta function. Eq. (23) can now be solved using familiar techniques. It is easiest to work in a shifted variable $\gamma \equiv \delta_c - \delta$ so that the finite boundary is at $\gamma = 0$.

The first step is to Fourier transform Eq. (23) in the variable γ (with conjugate ω). Thus we define the Fourier transform of the probability distribution

$$\tilde{\Pi}(\omega, S) = \int d\gamma \Pi(\gamma, S) e^{i\omega\gamma}. \quad (24)$$

This gives an equation for the transform

$$\frac{\partial \tilde{\Pi}}{\partial S} = -\frac{\omega^2}{2} \tilde{\Pi} \quad (25)$$

with solution

$$\tilde{\Pi}(\omega, S) = c(\omega) \exp\left(\frac{-\omega^2}{2} S\right). \quad (26)$$

The boundary condition at $\gamma = 0$ ($\delta = \delta_c$) guarantees that $c(\omega)$ is an odd function, so

$$\Pi(\delta, S) = \int_0^\infty c(\omega) \sin(\omega\gamma) e^{-\omega^2 S/2} d\omega. \quad (27)$$

Applying the initial condition to Eq. (27) gives

$$c(\omega) = \frac{2}{\pi} \sin(\omega\gamma_0) \exp\left(\frac{\omega^2}{2} S_0\right), \quad (28)$$

where $\gamma_0 \equiv \delta_0 - \delta_c$. The final solution then follows by inverting the transform, so

$$\Pi(\gamma, S) = \frac{2}{\pi} \int_0^\infty \sin(\omega\gamma_0) \sin(\omega\gamma) \exp\left(\frac{-(S - S_0)}{2} \omega^2\right) d\omega, \quad (29)$$

from which

$$\Pi(\delta, S) = \frac{1}{\sqrt{2\pi\Delta S}} \left[\exp\left(-\frac{(\Delta\delta)^2}{2\Delta S}\right) - \exp\left(-\frac{[2(\delta_c - \delta_0) - \Delta\delta]^2}{2\Delta S}\right) \right], \quad (30)$$

where $\Delta S = S - S_0$ and $\Delta\delta = \delta - \delta_0$. The solution to Eq. (23) in Eq. (30) depends on the initial condition only with regard to the height of the barrier at δ_c in relation to the starting position at δ_0 . The first term in Eq. (30) is the Gaussian distribution that represents the points above threshold at S while the second term accounts for the trajectories that have been removed because they crossed above threshold at a filter scale $S' < S$ but would have crossed back below the threshold by S . Chandrasekhar (1943) gives an elegant solution to this ‘‘absorbing barrier’’ problem almost upon inspection,

exploiting the fact that random walks that hit the barrier have equal probability of continuing upward after their first encounter with the barrier as they do of continuing downward. After observing that, the solution above can be obtained using the method of images and subtracting the contribution from another source beginning at $\Pi(\delta, S = 0) = \delta_D(\delta - 2\delta_c)$, a shift of δ_c above the threshold. The derivation given here is most useful because it contains the logic needed to generalize the problem to more complicated processes and barriers.

The fraction of trajectories that have crossed above the threshold at or prior to some scale S is the complement of the Π distribution,

$$F(M) = 1 - \int_{-\infty}^{\delta_c} \Pi(\delta, S) d\delta = \operatorname{erfc}\left(\frac{\delta_c - \delta_0}{\sqrt{2}\Delta S}\right). \quad (31)$$

Taking $S_0 = 0$ and $\delta_0 = 0$ to indicate a starting value at very large smoothing scale, Eq. (31) is precisely the value given by Press & Schechter (1974), but without having to introduce an arbitrary factor of two to achieve the correct normalization. The second term in Eq. (30) that accounts for trajectories that crossed threshold at some large filter and then walked back back below threshold by S accounts for the probability missing from the Press & Schechter (1974) argument.

The differential probability for a mass element to be above threshold then follows by differentiation,

$$\begin{aligned} f(S|\delta_0, S_0)dS &\equiv \frac{dF}{dS}dS = \left(\int_{-\infty}^{\delta_c} \frac{\partial \Pi}{\partial S} d\delta \right) dS \\ &= \frac{1}{2} \left[\frac{\partial \Pi}{\partial \delta} \right]_{-\infty}^{\delta_c} dS \\ &= \frac{\delta_c - \delta_0}{\sqrt{2\pi}\Delta S^{3/2}} \exp\left[-\frac{(\delta_c - \delta_0)^2}{2\Delta S}\right] dS. \end{aligned} \quad (32)$$

Eq. (32) is the fundamental relation as it gives the probability of crossing a threshold given any starting point and any change in filtering scale ΔS . The fraction of mass in collapsed objects in a narrow range of masses is obtained by setting $S_0 = 0$ and $\delta_0 = 0$ and rewriting Eq. (32) in terms of the mass that corresponds to the variance $M(S)$,

$$\frac{dF}{dM} = \frac{1}{\sqrt{2\pi S}} \left. \frac{\delta_c}{S} \frac{dS}{dM} \right| \exp\left(-\frac{\delta_c^2}{2S}\right). \quad (33)$$

The mass function follows by using Eq. (17) and substituting $\sigma^2 = S$ results in

$$\frac{dn}{dM} = \sqrt{\frac{2}{\pi}} \frac{\rho_M}{M^2} \frac{\delta_c}{\sigma} \left| \frac{d \ln \sigma}{d \ln M} \right| \exp\left(-\frac{\delta_c^2}{2\sigma^2}\right). \quad (34)$$

Again, this is precisely the Press & Schechter (1974) mass function with no *ad hoc* factor of two.

Analytic mass spectra are often compared to simulation data without reference to specific power spectra by comparing the fraction of mass in collapsed objects per logarithmic interval in ν , $\nu f(\nu) \equiv dF/d \ln \nu$. For the standard excursion set theory,

$$f(\nu) = \sqrt{\frac{2}{\pi}} \exp\left(-\frac{\nu^2}{2}\right). \quad (35)$$

In Fig. 3, I compare the Press-Schechter/Excursion set predictions for fraction of mass in collapsed objects with the results of a suite of cosmological numerical simulations. While excursion set theory may explain the gross features of the mass spectrum of dark matter halos, it fails in its detail. The Press-Schechter/Excursion set relations predict too many low-mass halos and too few high-mass halos. Given the simplicity of the excursion set model described above, this is not surprising and the level of agreement provides encouragement that the excursion set model is a useful tool for understanding the gross features of halo abundance, formation, and clustering.

One detail not discussed so far is the assignment of mass to a particular filter radius R or variance S . As I have already mentioned, the Press & Schechter (1974) relation follows directly by assuming a window function that is a tophat in Fourier space, but such a window does not have a well-defined volume to associate with it. The method of circumventing this that is implemented most often is to simply use the formulas derived from the sharp k -space filtering assumption, but assign mass according to a configuration space tophat filter so that $M = 4\pi R^3/3\rho_M$ (though this is not the method used by Bond et al. 1991).

In the context of excursion set theory, the k -space tophat window function serves only to simplify the solution for $\Pi(\delta, S)$ [Eq. (30)] and the first barrier up-crossing distribution [Eq. (32)]. In principle, other windows can be used but the mathematics become significantly more complicated. This is because the steps are no longer independent so it is necessary to compute the entire trajectory at once to account for the correlations between the steps in

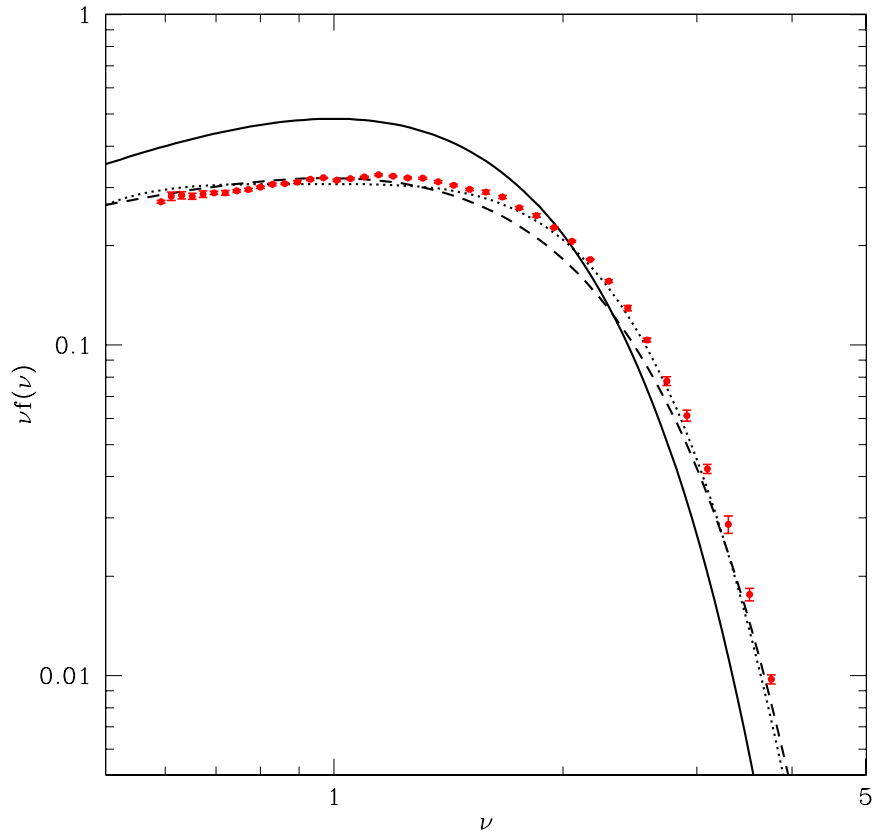


Figure 3: Collapsed mass fractions. The solid line represents the standard excursion set theory predictions. The dashed and dotted lines represent the improved fits of Sheth & Tormen (1999) and Jenkins et al. (2001) respectively. The points represent numerical data from a suite of N-body simulations kindly provided by J. L. Tinker.

smoothing scale. Bond et al. (1991) demonstrate the general procedure which amounts to generating a large number of solutions to a Langevin equation of random motion (*e.g.*, see Chandrasekhar, 1943) with a correlated stochastic force. Each solution yields a single trajectory of density at each value of the smoothing scale. The probability distributions are computed from the ensemble of trajectories. This procedure is potentially very complicated, time consuming, and it has the added drawback that it does not yield a closed-form solution for the $\Pi(\delta, S)$ or first up-crossing distributions. For these reasons, other filters are rarely discussed; however, it is important to keep in mind that the lack of correlations between different steps is not a general prediction of excursion set theory. Rather, this is a simplifying assumption of the most common implementation of excursion set theory.

5 Excursion Set Theory of the Spatial Bias of Dark Matter Halos

It has long been appreciated that within the context of cosmological structure formation theories, the clustering of dark matter halos differs from the overall clustering of matter (Kaiser, 1984; Efstathiou et al., 1988; Mo & White, 1996; Sheth & Tormen, 1999; Seljak & Warren, 2004). The excursion set formalism provides a neat framework with which to understand the relative clustering of halos. The argument is much the same as the peak-background split approach developed in Kaiser (1984), Efstathiou et al. (1988), and Cole & Kaiser (1989) and was expressed in the framework of the excursion set model by Mo & White (1996) as I outline below.

Consider the solution to the excursion set problem in Eq. (30). This gives the probability distribution of δ given that on smoothing scale S_0 , the smoothed density fluctuation is δ_0 . Notice that the important quantity is the relative height of the density threshold $\delta_c - \delta_0$ so that in regions with $\delta_0 > 0$ on large scales, trajectories are more likely to penetrate the barrier at δ_c and conversely for $\delta_0 < 0$. This means that Eq. (31) and Eq. (32) allow for the calculation of the mass function in regions with specific large-scale density fluctuations.

The fraction of mass in collapsed halos of mass greater than M in a region that has a smoothed density fluctuation δ_0 on scale S_0 (corresponding to mass

M_0 and volume V_0) is given by Eq. (31),

$$F(M|\delta_0, S_0) = \operatorname{erfc}\left(\frac{\delta_c - \delta_0}{2\Delta S}\right). \quad (36)$$

Notice that as the density of the region increases, F increases because smaller upward excursions are needed to cross the threshold. When $\delta_0 \rightarrow \delta_c$, $F \rightarrow 1$ because the entire region will then be interpreted as a collapsed halo of mass M_0 . The fraction of mass in halos with mass in the range M to $M + dM$ is

$$\begin{aligned} f(M|\delta_0, S_0) \left| \frac{dS}{dM} \right| dM &\equiv \frac{dF(M|\delta_0, S_0)}{dM} dM \\ &= \frac{1}{\sqrt{2\pi}} \frac{\delta_c - \delta_0}{\Delta S^{3/2}} \left| \frac{dS}{dM} \right| \exp\left[-\frac{(\delta_c - \delta_0)^2}{2\Delta S}\right] dM, \end{aligned} \quad (37)$$

so that regions with smoothed density δ_0 on scale S_0 contain, on average,

$$\mathcal{N}(M|\delta_0, S_0) dM = \frac{M_0}{M} f(M|\delta_0, S_0) \left| \frac{dS}{dM} \right| dM \quad (38)$$

halos in this mass range.

The quantity of interest is the relative over-abundance of halos in dense regions compared to the mean abundance of halos,

$$\delta_{\text{halo}}^{\text{L}} = \frac{\mathcal{N}(M|\delta_0, S_0)}{(dn(M)/dM)V_0} - 1, \quad (39)$$

where $dn(M)/dM$ is the mean number density of halos in a mass range of width dM about M from Eq. (34). The superscript L indicates that this is the overdensity in the initial Lagrangian space determined by the mass distribution at some very early time, prior to including the dynamical evolution of the overdense patch.

The relative overdensity of halos in large overdense and underdense patches is easy to compute. In sufficiently large regions, $S_0 \ll S$, $\delta_0 \ll \delta_c$. Expanding Eq. (39) to first order in the variables ξ_0/S and δ_0/δ_c gives a simple relation between halo abundance and dark matter density (see also Efstathiou et al., 1988; Cole & Kaiser, 1989)

$$\delta_{\text{halo}}^{\text{L}} = \frac{\nu^2 - 1}{\delta_c} \delta_0, \quad (40)$$

where $\nu = \delta_c/S^{1/2} = \delta_c/\sigma(M)$ as before. The overdensity in the initial Lagrangian space is proportional to the dark matter overdensity and is a function of halo mass through ν . The final ingredient needed to relate the abundance of halos to the matter density is a model for the dynamics that can map the initial Lagrangian-space to the final Eulerian space. Let V and δ represent the Eulerian space variables corresponding to the Lagrangian space variables V_0 and δ_0 . The final halo abundance is

$$\delta_{\text{halo}} = \frac{\mathcal{N}(M|\delta_0, S_0)}{(\text{dn}(M)/\text{d}M)V} - 1. \quad (41)$$

Mo & White (1996) give an extensive discussion of the mapping from Lagrangian to Eulerian coordinates and use a spherical collapse model to determine the appropriate mapping quantitatively. In the limit of a small overdensity $\delta_0 \ll 1$, $V \simeq V_0(1 + \delta)$, $\delta \simeq \delta_0$, and

$$\delta_{\text{halo}} = \left(1 + \frac{\nu^2 - 1}{\delta_c}\right) \delta \quad (42)$$

$$\equiv b_{\text{h}} \delta. \quad (43)$$

The halo overabundance is proportional to the matter overdensity and always has the same sense, and this proportionality is commonly referred to as the halo bias $b_{\text{h}} = (1 + [\nu^2 - 1]/\delta_c)$. Interestingly, Eq. (42) gives a mass scale at which halos are not biased with respect to the dark matter. If $\nu = 1$, or $\sigma(M) = \delta_c$ (signifying the typical mass scale collapsing at the present time), then $\delta_{\text{halo}} = \delta$. The mass at which this occurs is typically referred to as M_{\star} . Larger halos will have smaller values of $\nu = \delta_c/\sigma(M)$ because $\sigma(M)$ decreases with mass, so larger halos cluster considerably more strongly than the overall clustering of mass, while halos with $M < M_{\star}$ cluster more weakly than the overall mass distribution.

The large-scale halo bias relation of Eq. (42) is plotted as a function of scaled peak height ν , in Fig. 4. In that figure I also plot numerical results on the relative clustering bias of halo as well as improved fits for halo bias given by Sheth & Tormen (1999) and Seljak & Warren (2004). The fit of Sheth & Tormen (1999) can be motivated by excursion set theory with a modified form for the barrier (*e.g.*, Sheth et al., 2001; Sheth & Tormen, 2002). As with the mass function, the standard excursion set approach gives an understanding of the general features of the halo bias, but fails to reproduce the halo bias in detail.

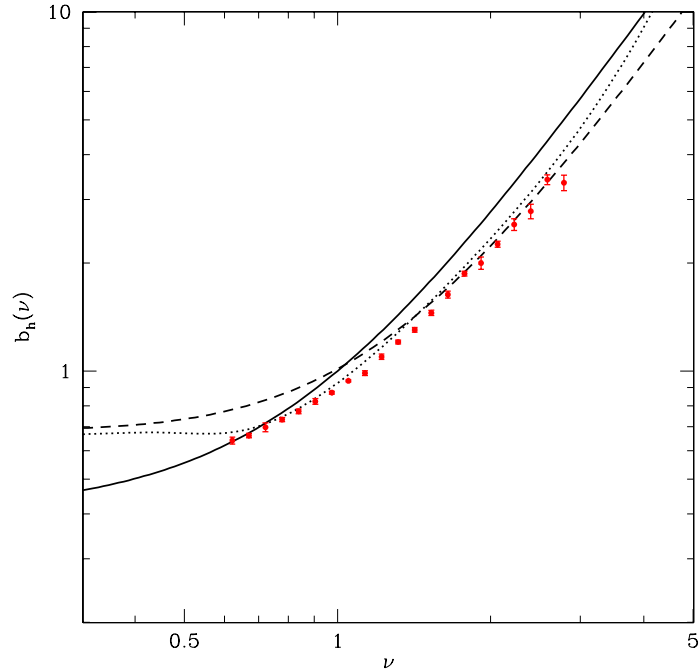


Figure 4: The large-scale bias of dark matter halos as a function of the scaled variable ν . The solid line gives the prediction of the standard Press-Schechter or excursion set theory in Eq. (42). The dashed line is a modified form for the bias that follows from a modified form for the barrier criterion given by Sheth & Tormen (1999). The dotted line represents an empirical fit to N-body simulation results given by Seljak & Warren (2004). The points represent numerical data from a suite of N-body simulations kindly provided by J. L. Tinker.

6 Halo Formation in the Excursion Set Theory

Excursion set theory is also a powerful formalism with which to study the formation history of halos. It is most natural to picture evolution occurring through the linear growth of the density field. In that way, the smoothed overdensity scales with time according to the linear growth factor $D(a)$. Writing the smoothed density field as a function of both the smoothing scale S and the cosmological expansion factor a , this evolution is $\delta(S, a) = D(a)\delta(S, a = 1)$. In the framework of excursion sets, predictions depend upon the density field in the ratio $\nu = \delta_c/\sigma(M)$ and it is often easier to envision the density field as fixed at $\delta(S) \equiv \delta(S, a = 1)$ and to consider the height of the critical density threshold as a function of time. In that way, collapse at a scale factor a' corresponds to the $a = 1$ density fluctuation penetrating a barrier of height $\delta_c(a') = \delta_c/D(a')$.

Bond et al. (1991) briefly discussed the utility of the excursion set approach for understanding the formation histories of halos. Lacey & Cole (1993) studied this problem in great detail and I largely follow their treatment in what follows. I will adopt the simplifying notation of Lacey & Cole (1993) and refer to the barrier height for collapse at a specific time as

$$\omega(a) \equiv \delta_c/D(a). \quad (44)$$

The variable ω indicates the time of the collapse through the linear growth function $D(a)$. Many of the insights into halo formation can be gleaned by considering the two-barrier problem, just as with halo bias in the previous section. Again following Lacey & Cole (1993), I also adopt a simplifying notation for the conditional probabilities of barrier crossings. I illustrate this notation by re-writing the two-barrier probability distribution already given in Eq. (32) and Eq. (37) as

$$f(S_2, \omega_2|S_1, \omega_1)dS_2 = \frac{1}{\sqrt{2\pi}} \frac{\Delta\omega}{\Delta S^{3/2}} \exp\left(-\frac{(\Delta\omega)^2}{2\Delta S}\right)dS_2, \quad (45)$$

where $\Delta\omega \equiv \omega_2 - \omega_1$ is the difference between the two barrier heights (assumed to be arbitrary with $\omega_2 > \omega_1$), $\Delta S \equiv S_2 - S_1$, and M_2 is the mass associated with the variance S_2 . The quantity $f(S_2, \omega_2|S_1, \omega_1)dS_2$ is the conditional probability that a trajectory pierces the barrier ω_2 in an interval of

width dS_2 about S_2 on the condition that the trajectory first pierces ω_1 at S_1 . As a further shorthand, I take $f(S_2, \omega_2)dS_2$ to denote the probability starting from a very large smoothing scale $S_1 = 0$, and $\omega_1 = 0$.

In this section and those that follow, the interpretation of Eq. (45) is different from that in § 4 and § 5. In those sections, the initial condition for the random walk was fixed by the large scale environment on some larger filtering scale S_1 . Here, the two barriers represent the critical density for collapse at two different times so the change in barrier height $\Delta\omega$ represents a shift in time.

6.1 The Conditional Mass Function

The most immediate quantity of interest is the conditional mass function. Given a halo of mass M_1 at time t_1 , one can compute the average manner in which this mass was partitioned among smaller halos at some earlier time $t_2 < t_1$ ($\omega_2 > \omega_1$). This is precisely the two-barrier problem. A halo of mass M_1 has its mass partitioned, on average, among a spectrum of halos at time ω_2 given almost directly from Eq. (45) (*e.g.*, Lacey & Cole, 1993; Somerville & Kolatt, 1999),

$$\frac{dn(M_2|M_1)}{dM_2} = \frac{M_1}{M_2} f(S_2, \omega_2|S_1, \omega_1) \left| \frac{dS_2}{dM_2} \right| dM_2. \quad (46)$$

The function $f(S_2, \omega_2|S_1, \omega_1)$ gives the probability of the second barrier crossing at a particular value of S_2 , while the factor M_1/M_2 converts this from a probability per unit mass of halo M_1 into the number of halos of mass M_2 .

Figure 5 shows conditional mass functions for standard CDM power spectra normalized such that $M_\star = 10^{13} h^{-1} M_\odot$ ($\sigma_8 \simeq 0.93$) for four halo masses at three different redshifts (all panels have final redshift at $z = 0$). The evolution toward increased fragmentation as the second epoch moves to higher redshifts is evident. Notice that more massive halos fragment into small sub-units more quickly. Also, notice that each conditional mass function goes toward an approximate power law as $M_2/M_1 \ll 1$. This can be understood directly from Eq. (5). Assume that the power spectrum is an approximate power law $S(M) \simeq \delta_c^2 (M/M_\star)^{-\beta}$ in the mass range of interest. In the limit of a large mass difference, $\Delta\omega/\Delta S \ll 1$ and $M_2/M_1 \ll 1$ and $dn/dM_2 \propto M_2^{-(4-3\beta)/2}$. Near M_\star , CDM-like power spectra vary slowly, with an effective power-law index near $\beta \approx 0.35$ giving $dn/dM_2 \propto M_2^{-3/2}$, which is approximately the power law shown in Figure 5.

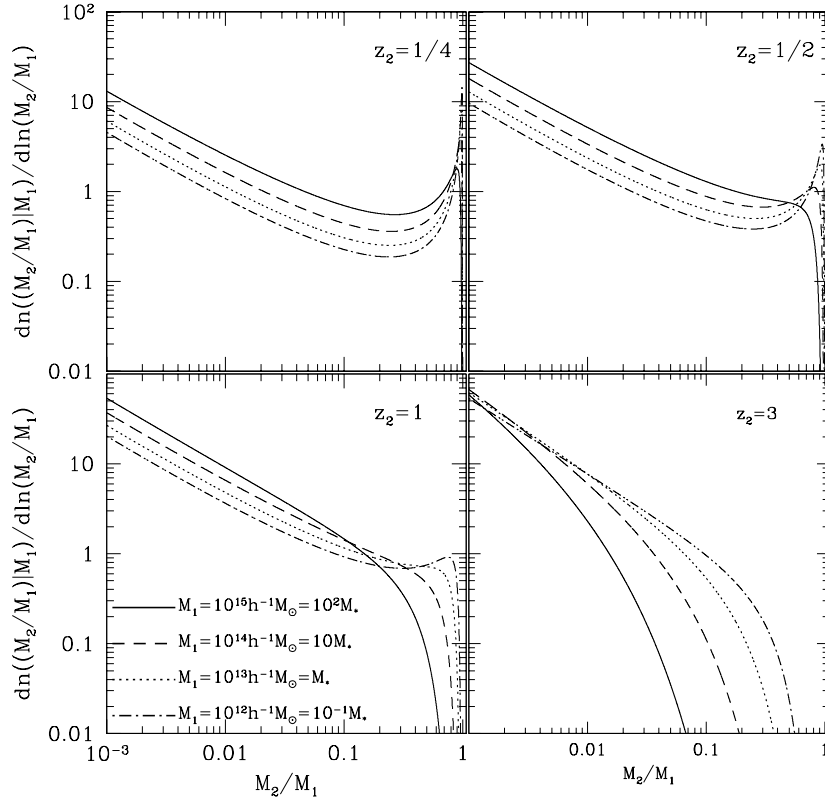


Figure 5: The conditional mass function. All panels refer to the conditional mass functions of halos fixed at $z = 0$ looking back toward higher redshifts as labeled in each panel. Four halo masses of interest are shown.

6.2 Halo Accretion Rates

The excursion set theory also provides a framework for computing mass accretion rates as well. The two-barrier problem of § 6.1 can be manipulated to give a mass accretion rate. Consider the probability of transitioning forward in time, from M_2 at barrier ω_2 to M_1 at ω_1 . Bayes' rule for combining probabilities gives the forward probability as (Lacey & Cole, 1993)

$$f(S_1, \omega_1 | S_2, \omega_2) dS_1 = \frac{f(S_2, \omega_2 | S_1, \omega_1) f(S_1, \omega_1)}{f(S_2, \omega_2)} dS_1 \quad (47)$$

$$= \frac{1}{\sqrt{2\pi}} \frac{\omega_1(\omega_2 - \omega_1)}{\omega_2} \left[\frac{S_2}{S_1(S_2 - S_1)} \right]^{3/2} \quad (48)$$

$$\times \exp \left(- \frac{(\omega_1 S_2 - \omega_2 S_1)}{2S_1 S_2 (S_2 - S_1)} \right) dS_1. \quad (49)$$

In language familiar to cosmology, $f(S_1, \omega_1 | S_2, \omega_2)$ is the posterior probability, $f(S_1, \omega_1)$ is the prior, and $f(S_2, \omega_2 | S_1, \omega_1)$ is the likelihood.

The instantaneous probability per unit shift in barrier height follows by taking $\Delta\omega = (\omega_2 - \omega_1) \rightarrow 0$ in Eq. (47), giving

$$\frac{d^2 R}{d\omega dS_1} = \frac{1}{\sqrt{2\pi}} \left[\frac{S_2}{S_1(S_2 - S_1)} \right]^{3/2} \exp \left[- \frac{\omega^2(S_2 - S_1)}{2S_2 S_1} \right], \quad (50)$$

from which the probability per unit change in mass $\Delta M = M_1 - M_2$, per unit time (or $d \ln a = H(a) dt$) is

$$\frac{d^2 R}{d \ln \Delta M d \ln a} = \sqrt{\frac{2}{\pi}} \frac{\Delta M}{M_1} \frac{\omega / \sigma(M_1)}{(1 - S_1/S_2)^{3/2}} \quad (51)$$

$$\times \exp \left[- \frac{\omega^2(S_2 - S_1)}{2S_1 S_2} \right] \left| \frac{d \ln \omega}{d \ln a} \right| \left| \frac{d \ln \sigma}{d \ln M_1} \right|. \quad (52)$$

The average rate of mass accretion per unit change in mass can be obtained by multiplying Eq. (51) by ΔM , while the average total mass accretion rate follows from multiplying Eq. (51) by ΔM and integrating over $\ln \Delta M$.

The excursion set accretion rates of halos in the standard Λ CDM cosmology are summarized in Fig. 6 and Fig. 7. The left panel Fig. 6 shows the probability for a particular fractional mass change as a function of the fractional mass change. The rate of accretion by small mass increments diverges.

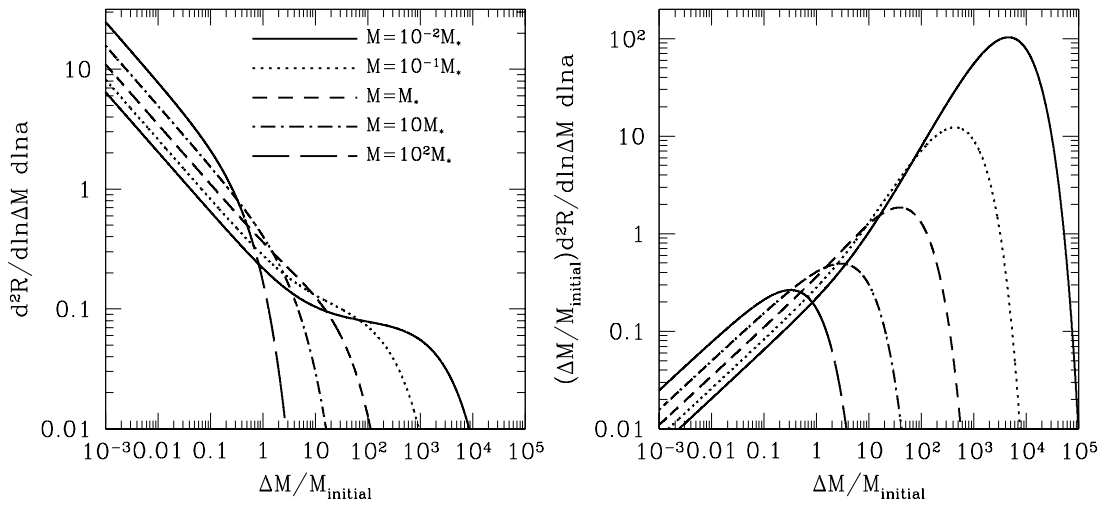


Figure 6: Halo accretion rates per logarithmic interval of mass change (following the similar plot by Lacey & Cole, 1993). The plots show the accretion rates per unit mass change for halos of five different masses (shown in the left panel) at $z = 0$. The left panel shows the probability for a change ΔM as a function of ΔM [Eq. (51)], while the right panel shows the fractional mass accretion rate given by $(\Delta M/M_2) \times d^2R/d\ln\Delta M d\ln a$.

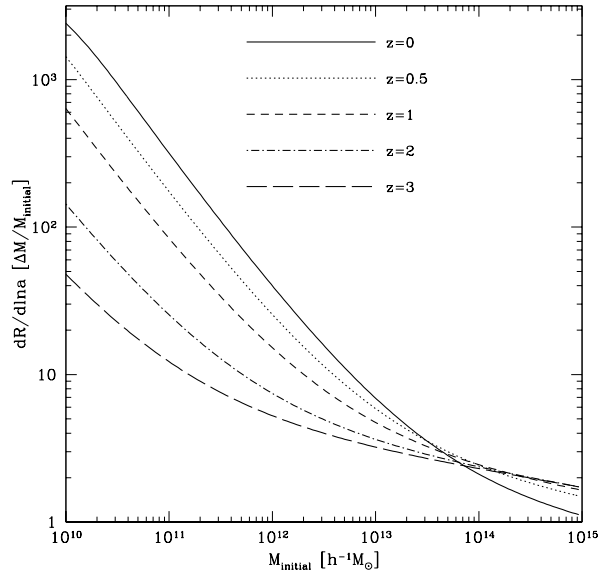


Figure 7: Total halo mass accretion rates in units of halo mass and as a function of halo mass at four different redshifts.

However, the average rate of mass increase (in the right panel of Fig. 6) converges and is dominated by the less frequent high-mass mergers. Notice in particular that low-mass halos increase their masses very quickly via mergers with halos larger than themselves while halos with $M > M_*$ experience only infrequent mergers with halos larger than themselves.

The total mass accretion rate given by integrating Eq. (51) over $\ln \Delta M$ is shown in Fig. 7 for various redshifts as a function of halo masses. Fig. 7 shows explicitly that low-mass halos should be expected increase their mass many times over in a Hubble time. The standard interpretation of these facts is that low-mass halos ($M < M_*$) should be expected to increase their masses by mergers with halos larger than themselves, while high-mass halos ($M > M_*$) typically absorb smaller halos and increase their masses relatively slowly.

6.3 Halo Formation Times

It is often useful to have a sense of a time by which a halo acquired most of its mass. For example, one may be modeling galaxies and may try to estimate stellar evolution histories within a particular halo. Several definitions of halo formation time exist. An intuitive definition is the time that a halo first acquires half of its final mass because once a progenitor of a halo has achieved this threshold it can uniquely be identified as the main progenitor of the final object. Consider the formation time given by this definition ω_F or a_F .

It is not trivial to predict this quantity using excursion set theory by considering the two-barrier problem as before. The reason is simple. Consider the formation of a halo of mass M_1 at time ω_1 . The probability of crossing the threshold to some threshold $> S_2 = S(M_1/2)$ at some time ω_2 gives only the probability per unit mass that the halo has some progenitor with mass $M_2 < M_1/2$ at time ω_2 . It does not guarantee that this is the mass of the most massive of all of the subunits that merged to form the halo of mass M_1 at ω_1 . Lacey & Cole (1993) circumvent this difficulty by giving an approximate counting argument for the formation time that I now review.

First, the results of § 6.2 give the number of halos of mass M_2 at time t_2 that are incorporated into halos of mass M_1 at $t_1 > t_2$ as

$$\frac{d^2 n}{dM_2 dS_1} = \frac{dn(M_2)}{dM_2} f(S_1, \omega_1 | S_2, \omega_2). \quad (53)$$

So long as $M_1 \geq M_2 > M_1/2$ each trajectory must connect unique halos because there cannot be two paths each of which contain more than half of the final mass. However, it is possible that a halo of mass M_1 at t_1 has no progenitor of mass $> M_1/2$ at time t_2 . The probability that a halo of mass M_1 at t_1 has a progenitor in the mass range $M_1 \geq M_2 > M_1/2$ at time t_2 is then given by the ratio of halos that evolve to a halo of mass M_1 relative to the total number of halos of mass M_1 ,

$$\frac{dP}{dM_2} = \frac{[dn(M_2)/dM_2]f(S_1, \omega_1|S_2, \omega_2)}{[dn(M_1)/dM_1]||dS_1/dM_1|^{-1}}. \quad (54)$$

Using Bayes' rule again and the definitions of the mass functions gives

$$\frac{dP}{dM_2} = \left(\frac{M_1}{M_2}\right) f(S_2, \omega_2|S_1, \omega_1) \left| \frac{dS_2}{dM_2} \right|. \quad (55)$$

The cumulative probability of a formation time prior to time t_2 is then the integral

$$P(t_F < t_2) = P(\omega_F > \omega_2) = \int_{S_1}^{S_2=S(M_1/2)} \left(\frac{M_1}{M_2}\right) f(S'_2, \omega_2|S_1, \omega_1) dS'_2, \quad (56)$$

and the differential probability can be obtained by differentiating with respect to ω_F or t_F .

Formation time distributions computed from Eq. (56) are shown in Fig. 8 for a variety of halo masses at $z = 0$ ($a = 1$, $\omega_F = \delta_c \simeq 1.69$). The most obvious feature of formation times is that small halos form early and large halos form relatively late in accordance with our general expectation in hierarchical models of structure formation. In the next section, I discuss halo formation times in the context of halo merger trees.

7 Halo Merger Trees

The probability of first up-crossing at a second barrier given a particular starting point is given by the solution to the two-barrier problem in Eq. (45). This relation has been repeated several times throughout these notes in several forms because it is the fundamental relation on which most physical results are based. In the preceding sections, I have applied this formula to derive relations about various aspects of halo fragmentation and formation

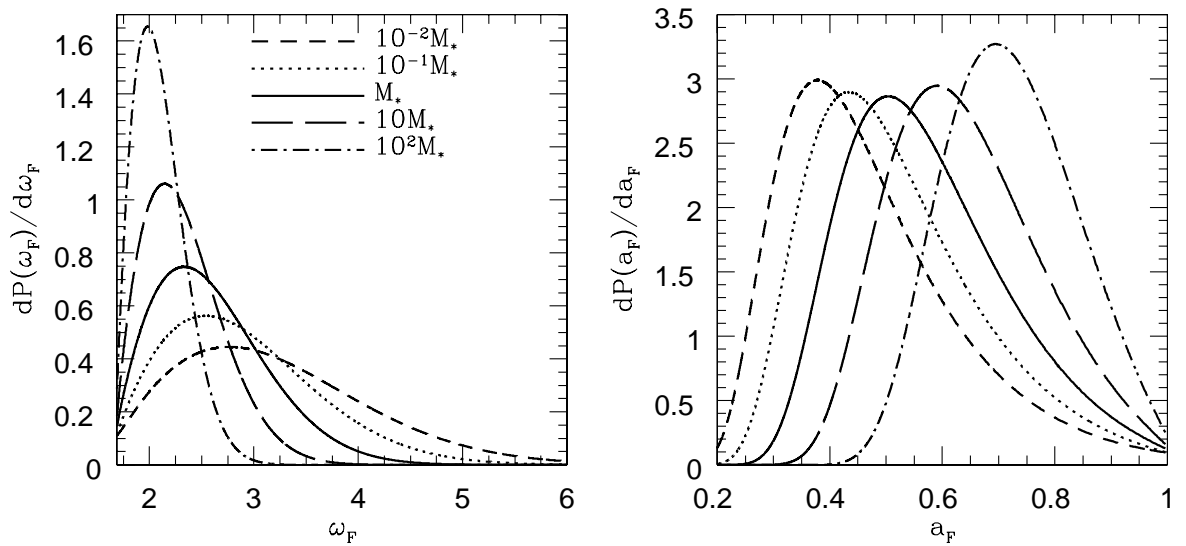


Figure 8: The probability distributions for formation times in the standard Λ CDM cosmology with a scale-invariant primordial power spectrum normalized to $\sigma_8 = 0.93$, so that $M_* = 10^{13} h^{-1} M_\odot$. The left panel shows the distribution as a function of threshold height $dP(\omega_F)/d\omega_F$ while the right panel shows the probability distribution of formation scale factors $dP(a_F)/da_F$.

over time. So far, these quantities have been averages (as in § 6.1 and § 6.2) or probability distributions (as in § 6.3). However, as Lacey & Cole (1993) describe, the interpretation of Eq. (45) as a probability for a transition from one barrier to another means that one should be able to draw specific fragmentation probabilities from this distribution repeatedly for a number of time intervals $\Delta\omega_i$, and thereby reconstruct individual trajectories. This enables one to follow the fragmentation of halos on an object-by-object basis. This is the logic behind the algorithm for the generation of Monte Carlo merger trees described by Lacey & Cole (1993, see also earlier methods in Cole & Kaiser 1988; Cole 1991).

The trajectories $\delta(S)$ generally have structure on arbitrarily small scales corresponding to mergers with very small halos. This is a restatement of the divergence of the mean number of transitions with small mass changes shown in the left panel of Fig. 6. Consequently, it is necessary to examine trajectories with a particular resolution in order to “smooth over” the mergers with numerous tiny halos. In practice, almost every physical application has a minimum mass scale of interest M_{\min} , so it is natural to set the resolution with which trajectories are computed according to this minimum scale. Consider Eq. (45) in the limit $\Delta\omega/\sqrt{\Delta S} \ll 1$. This gives a transition probability $f = \Delta\omega/(\sqrt{2\pi}\Delta S^{3/2})$, that is directly proportional to the time interval $\Delta\omega$. Lacey & Cole (1993) interpreted this as indicative of a probability that is due to a single, improbable merger event. This can be used to motivate a particular choice of step-size $\Delta\omega$ that sets the resolution of the trajectory.

First, consider making the change of variable to $u \equiv \Delta\omega/\sqrt{\Delta S}$ in Eq. (45). This converts the probability distribution to a Gaussian in the variable u with a mean of zero and a unit variance. Of course, the probability distribution is one-sided in that it is subject to the constraint $u \geq 0$. To resolve individual, binary mergers of a parent halo of mass M with a merging halo at the threshold M_{\min} the step-size should obey

$$\Delta\omega \lesssim \sqrt{\left| \frac{dS(M)}{dM} \right| M_{\min}}, \quad (57)$$

so that these mergers are in the binary regime. Authors often parameterize this guideline and set $\Delta\omega = f_{\text{step}}\sqrt{|dS/dM|M_{\min}}$. This makes a transition with $\Delta M \geq M_{\min}$ a rare event and places the transition probability in the binary regime. In particular, the probability for a transition with $\Delta M \geq$

M_{\min} is

$$\begin{aligned}
P(> \Delta M) &= \frac{2}{\sqrt{\pi}} \int_0^{f_{\text{step}}/\sqrt{2}} \exp(-y^2) dy \\
&= \text{erf}(f_{\text{step}}/\sqrt{\pi}) \\
&\approx \sqrt{\frac{2}{\pi}} f_{\text{step}},
\end{aligned} \tag{58}$$

as before, where the last step assumes $f_{\text{step}} \ll 1$. The choice of f_{step} is motivated by the need to resolve mergers of objects of mass M_{\min} , driving f_{step} toward small values, and the desire to spend as little effort as possible computing the probabilities for transitions with $\Delta M < M_{\min}$, driving f_{step} toward large values. Furthermore, as I discuss below Somerville & Kolatt (1999) advocate $f_{\text{step}} \lesssim 0.3$ in order to guarantee accuracy down to M_{\min} . Typical values are $f_{\text{step}} \lesssim 0.1$.

The Lacey & Cole (1993) algorithm for generating merger histories is then as follows. First, determine the appropriate timestep. Second, select a transition ΔS from the probability distribution of Eq. (45) and invert the $S(M)$ relation to obtain the change in mass ΔM and the new main progenitor mass $M' = M - \Delta M$. One then repeats this procedure at the new values of ω and $S(M')$ in order to determine the next fragmentation of the main progenitor. The trajectory for the main progenitor, defined as the most massive progenitor at each timestep according to this algorithm, may form the trunk of a “merger tree.” All of the merging halos of mass ΔM have prior fragmentation histories of their own. For each mass ΔM above the threshold M_{\min} , one can generate a history for the infalling “branch” on the tree using the same algorithm. Mergers with halos of mass $\Delta M < M_{\min}$ are regarded as “accreted mass,” but note that in the excursion set theory all mass merges in halos and none is ever truly diffuse accretion (this statement is specific to spherical collapse, meaning a barrier that is a constant function of S). This nomenclature is simply the convention used to distinguish mergers above the threshold from mergers below threshold. This process must be repeated numerous times in order to sample the variety of ways in which a halo of a fixed mass at a fixed time might build up its mass. It is conventional to refer to each individual tree generated in this way as a particular *realization* in an ensemble of merger histories.

This algorithm for generating Monte Carlo merger trees is convenient because of its simplicity. Unfortunately, while this algorithm conserves mass

by construction, it overpredicts the number of progenitor halos with masses $M > M_{\min}$ at previous timesteps relative to the analytic distribution of Eq. (46) as was emphasized by Somerville & Kolatt (1999, see also Sheth & Lemson 1999). In other words, the Monte Carlo procedure does not lead to a mean population of halos at high redshift that is consistent with the excursion set relations of the previous section. Somerville & Kolatt (1999) suggested two very plausible sources for this discrepancy. The first is that after choosing the first mass ΔM from Eq. (45), the mass of the second body in the merger is forced to be $M' = M - \Delta M$ in order to conserve mass without regard to the probability of a transition to the mass M' . This drives an overabundance of high-mass halos because all of the remaining mass is forced into a halo of mass M' . The second source stems from the fact that the simple algorithm above largely neglects accretion with transitions $\Delta M < M_{\min}$ when the probability for such a transition becomes infinitely large as $\Delta M \rightarrow 0$. While Somerville & Kolatt (1999) do not present a rigorous demonstration of a self-consistent algorithm, they give a qualitatively well-motivated algorithm that reproduces analytic halo conditional mass functions at high redshift very well as I now summarize. A successful algorithm that is, in practice, very similar to that of Somerville & Kolatt (1999) is developed through Sheth (1996), Sheth & Pitman (1997), and Sheth & Lemson (1999), though this approach also lacks any rigorous support other than that it is exact for an uncorrelated density field.

The Somerville & Kolatt (1999) algorithm begins in the same manner as the Lacey & Cole (1993) procedure. First, choose a timestep corresponding to the desired mass resolution. At each timestep choose a transition ΔS from Eq. (45) and convert it to a mass change ΔM . If $\Delta M < M_{\min}$, remove it from further consideration and regard it as diffuse accretion. If $\Delta M \geq M_{\min}$ treat it as a progenitor halo that has merged. Next, update the remaining mass to $M_{\text{rem}} = M - \Delta M$. The algorithm now deviates from the binary split procedure of Lacey & Cole (1993). Instead of requiring a second member of the merger to be a halo of mass $M' = M_{\text{rem}}$, the Somerville & Kolatt (1999) algorithm allows for an arbitrary number of progenitors each of which is chosen from Eq. (45) as well as an arbitrary amount of accreted mass. The next step then, is as follows. If $M_{\text{rem}} > M_{\min}$, choose another transition and get the new mass change $\Delta M'$. If $\Delta M' > M_{\min}$, treat it as a merger and if $\Delta M' < M_{\min}$, treat it as accretion. Update M_{rem} by subtracting $\Delta M'$. This procedure is then repeated until $M_{\text{rem}} \leq M_{\min}$ at which point the remaining mass is regarded as diffuse accretion. This produces a list of progenitors after

a single timestep. To fill out the tree, one applies this procedure with new timesteps to all the progenitors in the list and so on, recursively building a merger tree. The tree is of finite extent because each branch off of the tree terminates when all mass enters in units that are $< M_{\min}$, so that each unit is regarded as accreted material.

An example of mass accretion histories for main progenitors (the most massive progenitor at each timestep) computed according to this merger tree prescription is shown in Fig. 9. The large vertical jumps correspond to very sudden increases in mass due to (perhaps multiple) major mergers. The variety of different paths to the same final mass is evident. Also clear in Fig. 9 is the fact that smaller halos acquire their masses relatively earlier than larger halos, a picture that is consistent with the results shown in Fig. 6. Formation times are also easy to compute directly from these merger histories. The distribution of formation times among Monte Carlo realizations is shown in Fig. 10. Also shown in Fig. 10 are the formation time distributions from § 6.3, which appear to be in reasonable agreement (Note that the agreement here is better than that shown in Lacey & Cole 1993 due to the use of the Somerville & Kolatt 1999 algorithm rather than the binary split algorithm).

Merger trees also give a wealth of information on how the mass is acquired by the parent halos. Some properties of the distribution of all mergers are extremely simple. Consider the transition probability in the binary regime and in the regime $\Delta M \ll M$ so that the merging object is much smaller than the main progenitor with which it is merging. In this case, the transition probability is $f \sim [\Delta\omega/(\sqrt{2\pi}|dS(M)/dM|)]\Delta M^{-3/2}$. As such, the average mass fraction that is accreted in units in a logarithmic interval $\ln(\Delta M)$ is varies as $dF/d\ln(\Delta M) \sim [\Delta\omega/(\sqrt{2\pi}|dS/dM|^{1/2})]\Delta M^{1/2}$ for all timesteps. This requires only that the probability be in the binary regime and the mass change be small. Integrating over all time, the full tree has this property as well with a deviation at $\Delta M \sim 0.1M$ necessitated by mass conservation. The total mass accreted in units of mass ΔM per logarithmic interval $d\ln(\Delta M)$ integrated over the entire history of 1000 realizations of the merger history of an M_* halo is shown in Fig. 11. The scaling $dF/d\ln(\Delta M) \propto \Delta M^{1/2}$ at $\Delta M \ll M$ is evident. Integrating over $\ln(\Delta M)$ gives $F = 1$ because all mass is acquired in the form of halos of a particular mass in the excursion set model.

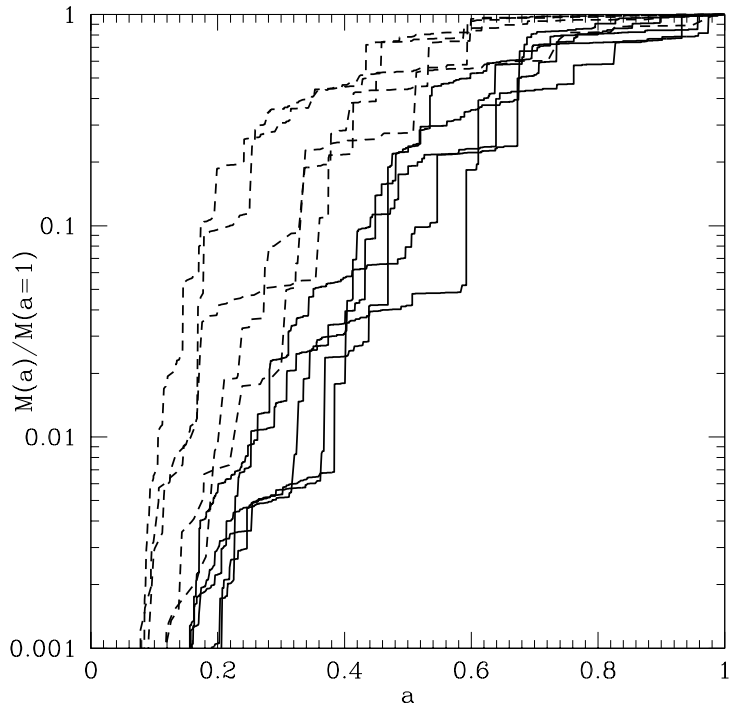


Figure 9: Ten examples of mass accretion histories as a function of cosmological scale factor for main progenitors. These histories were generated using the Monte Carlo merger history method based on excursion set theory as described in the text. The solid lines correspond to a large cluster halo with a mass of $10^{15} h^{-1}M_{\odot}$ at $z = 0$ ($a = 1$). The dashed lines correspond to a Milky Way-sized halo with mass $M(a = 1) = 10^{12} h^{-1}M_{\odot}$.

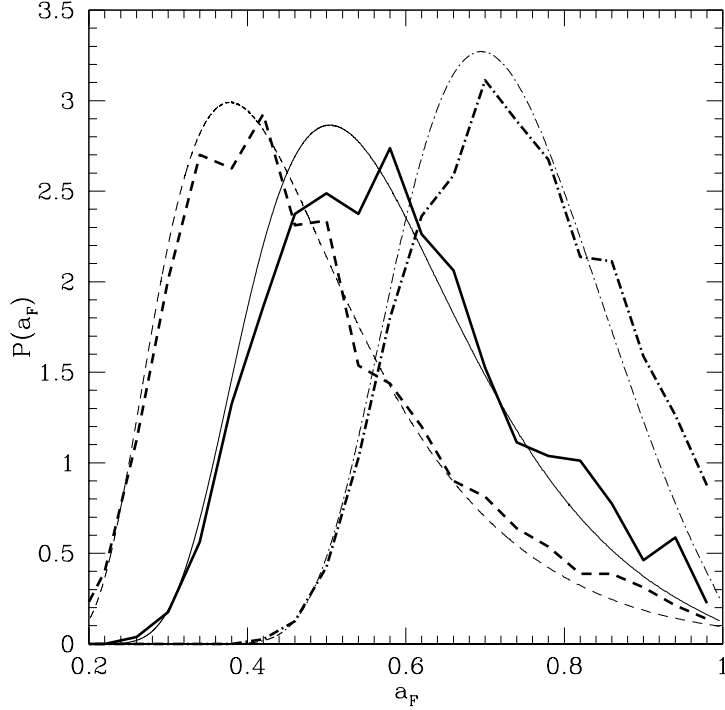


Figure 10: Halo formation times computed from the Monte Carlo merger tree algorithm compared to the closed form distribution of formation times given in § 6.3. The dashed lines correspond to halos of mass $10^{11} h^{-1}M_{\odot}$, the solid lines correspond to halos of mass $10^{13} h^{-1}M_{\odot} = M_{*}$, and the dash-dot lines correspond to halos of mass $10^{15} h^{-1}M_{\odot}$. The thin, smooth lines are the analytic predictions while the thick lines are the results 1000 realizations of the Monte Carlo procedure.

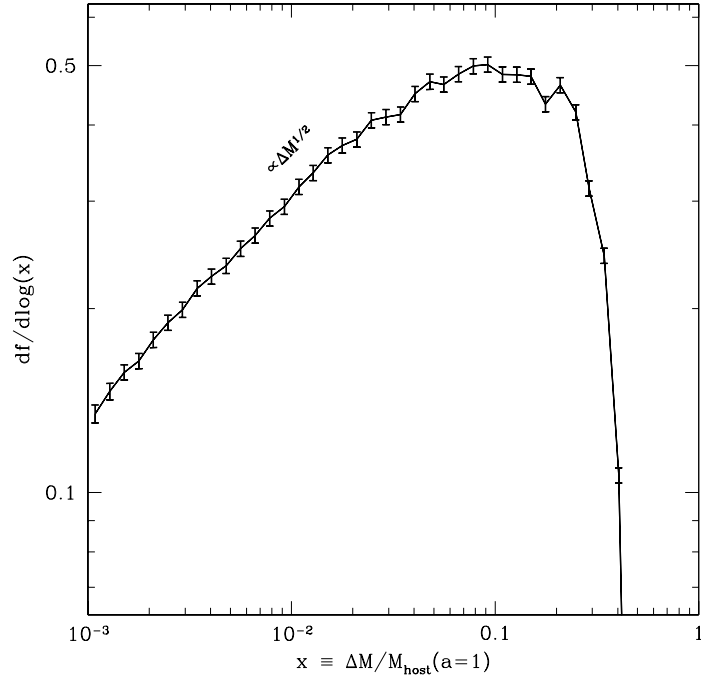


Figure 11: The total fraction of a host halo mass at $a = 1$ accreted in units of size $\Delta M/M$ per logarithmic interval $d \ln(\Delta M)$, $dF/d \ln(\Delta M)$. The result shown is from 1000 merger histories of a halo with mass $10^{13} h^{-1} M_{\odot} = M_{\star}$ at $a = 1$.

8 Beyond the Simple Excursion Set Approach

In the proceeding sections, I have reviewed the simplest implementation of the excursion set approach to halo formation. While this approach provides valuable insight into the influence of the statistical properties of the density field on the distribution and formation of halos, in its detail it is known to have a number of shortcomings that render it a less than ideal tool for applications where precision is required (Lacey & Cole, 1994; Gelb & Bertschinger, 1994; Jing, 1998; Tormen, 1998; Sheth & Tormen, 1999; Somerville & Kolatt, 1999; Jenkins et al., 2001; Sheth & Tormen, 2002, are a sample of numerous studies pointing out various issues). I will discuss briefly some of these shortcomings and some insights into the physical origin of these shortcomings in what follows. One point that is important to emphasize is that the excursion set approach is itself an approximation that neglects the details of nonlinear dynamics; however, the predictions discussed in the previous sections largely result from making several further assumptions that are motivated primarily by simplicity and may not be the basis of the most accurate implementation of excursion set theory.

8.1 Ellipsoidal Collapse and Nontrivial Barrier Shapes

One way in which the excursion set predictions are simplified is to assume that collapse and virialization of a halo occurs whenever the smoothed density exceeds a critical value δ_c , that is independent of any further details of the density field. Even some of the gross qualitative aspects of excursion set theory no longer hold when this simple form for the barrier no longer holds.

Following Sheth (1998), it is instructive to examine a simple toy example such as the linear barrier where the threshold increases with the variance $\delta'_c(S) = \delta_c + \beta S$ (constructed so that it can be easily solved). In this case the barrier recedes from the line $\delta = 0$ at a “rate” β . Solving for the first crossing distribution of this barrier is equivalent to solving for the first crossing distribution of a constant barrier where the transition probability causes trajectories to “drift” away from the barrier at a rate β . In this case, we can revisit the logic that led to Eq. (22) but note that the mean transition should be $\langle \Delta \delta \rangle = -\beta \Delta S$ so that Eq. (23) is replaced by

$$\frac{\partial \Pi}{\partial S} = \frac{1}{2} \frac{\partial^2 \Pi}{\partial \delta^2} + \beta \frac{\partial \Pi}{\partial \delta}. \quad (59)$$

The boundary conditions and the initial condition are the same as before.

The solution to Eq. (59) can be greatly simplified by making the transformation $\Pi = U \exp(\beta[\gamma - \beta S/2])$ where $\gamma \equiv \delta_c - \delta$ as in § 4. In that case $U(S, \gamma)$ satisfies

$$\frac{\partial U}{\partial S} = \frac{1}{2} \frac{\partial^2 U}{\partial \gamma^2}, \quad (60)$$

which is the diffusion equation with no drift term, and the conditions

$$U(S = 0, \gamma) = \delta_D(\gamma - \delta_c) \exp(-\beta\gamma) \quad (61)$$

and

$$U(S, \gamma = 0) = 0 \quad (62)$$

Following § 4, this gives the result

$$\Pi(S, \delta) = \frac{\exp(-\beta[\beta S/2 + \delta])}{\sqrt{2\pi S}} \left[\exp\left(-\frac{\delta^2}{2S}\right) - \exp\left(-\frac{[2\delta_c - \delta]^2}{2S}\right) \right]. \quad (63)$$

From Eq. (63), the fundamental relation for the probability for a mass element to be above threshold at a variance between S and $S + dS$ is

$$f_{\text{lin}}(S|\delta_0 = 0, S_0 = 0)dS = \frac{\delta_c}{\sqrt{2\pi}S^{3/2}} \exp\left(-\frac{[\beta S + \delta_c]^2}{2S}\right). \quad (64)$$

From this solution to the simple linear barrier a mass function can be derived in the usual way.

It is useful to note a few things from this example. First, consider a mass function arising from Eq. (64). For $S \ll \delta_c/\beta$, the mass function will have an exponential cut-off for high-mass (low- S) objects as before. Additionally, for $S \gg \delta_c/\beta$ the mass function will feature an exponential suppression of low-mass object as well. This is due to the fact that the barrier increases in height as S while the standard deviation of the walk increases only as \sqrt{S} so that the barrier becomes harder and harder to pierce at high S . In contrast, the constant barrier will always be crossed because the standard deviation of the walk \sqrt{S} , always becomes much larger than the barrier height as S increases. This leads to a second interesting feature. Integrating Eq. (64) over all S gives the total fraction of mass in bound halos as $F = \exp(-2\beta\delta_c) < 1$. The statement that all matter is bound into halos is not generally true in the excursion set approach, but is a result of specific barrier shapes.

The third interesting aspect is that the variance S is a function of redshift. This means that barriers at different times will have different shapes so that, for example, bias relations, conditional mass functions, and merger tree transitions will not result from the solution of the same, simple two-barrier problem. In the case of the linear barrier, this can be overcome by a simple rescaling of the variables as before, but in general this represents a significant complication. It is necessary to solve the boundary value problem for each initial condition and boundary condition of interest. There are other interesting features of varying barrier shapes, perhaps halo fragmentation (*e.g.*, Sheth & Tormen, 2002), but this gives a flavor that many of the standard statements regarding excursion set theory are actually statements that are limited to excursion sets plus some simplifying assumptions.

In fact, nontrivial barriers may play an important practical role in understanding things like the mass function and bias of halos. Sheth & Tormen (1999) noted that the GIF simulations obeyed a mass function where the fraction of mass in collapsed objects is modified from Eq. (35) to

$$f_{\text{ST}}(\nu) = A \sqrt{\frac{2a}{\pi}} \left(1 + \frac{1}{(\sqrt{a\nu})^{2p}} \right) \nu \exp(-a\nu^2/2), \quad (65)$$

with $a = 0.707$, $p = 0.3$, and $A = 0.322$ in order to guarantee that all mass is bound into halos of some mass. This is the form shown in Fig. 3 and it clearly represents a major improvement over the simple excursion set/Press-Schechter mass function. Sheth & Tormen (1999) also showed that this form translated into a much improved model for halo bias (using the usual logic) as shown in Fig. 4.

Subsequently, Sheth et al. (2001) and Sheth & Tormen (2002) discussed how the collapse fraction in Eq. (65) is very similar to the collapse fraction one would derive from of an excursion set model with a nontrivial barrier the form of which is motivated by considering the ellipsoidal, rather than spherical, collapse of structures. In general, integrating the full details of ellipsoidal collapse into the excursion set formalism is quite complicated, but these authors greatly simplified the problem by considering the barrier that results from the mode of the distributions for ellipticity and prolateness of overdense patches (see Bond & Myers, 1996; Sheth et al., 2001; Sheth & Tormen, 2002, for details). In short, the simplification stems from assigning overdense patches only a single shape rather than a distribution of possible

shapes. The resulting barrier is (Sheth et al., 2001; Sheth & Tormen, 2002)

$$\delta_c^{\text{ell}} = \delta_c(1 + \beta\nu^{-\gamma}), \quad (66)$$

where $\beta \approx 0.47$ and $\gamma \approx 0.62$ are determined by considering the evolution of an ellipsoidal density perturbation rather than a perfectly spherical density perturbation.

Notice that the ellipsoidal collapse barrier of Eq. (66) is higher for low-mass (low- ν) objects. The physical reasoning for this is that low-mass objects typically exhibit greater ellipticity (*e.g.*, Bond & Myers, 1996; Sheth et al., 2001) and are more prone to disruption by tidal interactions so that their densities must be higher in order to overcome this. Notice that one of the primary deficiencies of the constant-barrier excursion set mass function is that it predicts considerably too many low-mass halos (see Fig. 3). As the barrier is higher for higher S (lower mass), one should expect a reduction in low-mass halos relative to the standard excursion set mass function and this is precisely what is shown in Fig. 3. Finally, Sheth & Tormen (2002) showed that the ellipsoidal model still failed to model accurately conditional mass functions at small lookback times and large mass ratios and the number densities of halos in very overdense regions. This failure leads to the next simplification of the excursion set approach.

8.2 Correlations Between Scales

In § 4, I noted that the use of the sharp k-space filter represents something of a problem because the sharp k-space window is difficult to associate with any particular mass. Once some method for assigning mass to a filter is decided upon, the use of the sharp k-space filter also has an important implication for the properties of halos. In the case of a sharp k-space window function, the transitions between different smoothed densities are independent Gaussian random variables as in Eq. (20). This implies that the formation histories of halos are completely uncorrelated with their local environments because in the excursion set formalism a halo of mass M has $\delta(S) = \delta_c$ at $S = S(M)$ while all steps away from this value are independent of each other.

Though the effects are small, several studies have recently pointed out that the formation histories of halos in cosmological numerical simulations are correlated with their environments (*e.g.*, Sheth & Tormen, 2004; Gao et al., 2005; Wechsler et al., 2006). The implication of these studies is that

correlations between scales cannot be neglected in applications where precision is required.

Along these lines Sheth & Tormen (2002), attempted to determine whether or not their conditional mass functions were in error because of an incomplete treatment of ellipsoidal collapse and concluded that a more detailed treatment of ellipsoidal collapse could not explain the failures of their model to predict conditional mass functions and density-dependent mass functions. They reasoned that because the worst failures occurred in high-density regions and for conditional mass functions at small lookback times and for high mass ratios, the deficiency may be due to a neglect of correlations between different scales. The reasoning follows because at high mass ratios and small lookback times for the conditional mass functions or for mass functions in high density regions, the differences in smoothing scales between the overdense region or parent halo, and the smaller structures within it are small. However, in the regime where mass differences and lookback times are large the smoothing scales involved are quite different so it might not be surprising for correlations over very different scales to be different.

Correlations between scales can be incorporated into the excursion set approach simply by modifying the window function. Any window function other than a sharp k-space window will result in walks where all steps are correlated. In the case of correlated walks, the $\int f(S)dS$ must be computed by integrating numerically a Langevin equation as described in Bond et al. (1991). To my knowledge, the issues mentioned above have not been addressed in this way and it is unclear whether the excursion set approach with correlated walks can eliminate these discrepancies or whether these discrepancies arise due to the nonlinear evolution during halo formation. Such an investigation is well beyond the scope of these lectures.

8.3 The PINOCCHIO Algorithm

In closing, I would like to point toward another tool for estimating halo mass functions and formation histories quickly and accurately. This is the publicly-available PINOCCHIO code developed by P. Monaco and collaborators Monaco et al. (2002a,b); Taffoni et al. (2002) which can be obtained from ¹. The great value of the PINOCCHIO code is that it is considerably less computationally expensive than a cosmological N-body simulation but predicts halo properties

¹URL <http://adlibitum.oats.inaf.it/monaco/Homepage/Pinocchio/>

and formation histories that are in excellent agreement with N-body results relative to the simple excursion set approach.

Briefly, the PINOCCHIO code uses an algorithm for identifying halos and halo properties such as mass, velocity, angular momentum in particular realizations of the linear density field. The PINOCCHIO code also contains a parameterized algorithm for building filamentary structures in the density field and for generating the merging histories of halos. PINOCCHIO creates a particle-based realization of the linear density field in a manner similar to standard N-body simulations. PINOCCHIO then computes the approximate evolution of mass elements using a particular truncation of third order Lagrangian perturbation theory (for example, first order Lagrangian perturbation theory constitutes the well-known Zel'dovich Approximation used to initialize most N-body simulations). As PINOCCHIO is perturbative, the computation progresses at a fraction of the computational effort of an N-body simulation. PINOCCHIO groups mass elements together into halos using an orbit-crossing condition. When the orbits of two mass elements coincide, Lagrangian perturbation theory breaks down because the mapping from Eulerian position to Lagrangian position becomes multi-valued and the density is infinite. At this point, the mass elements are grouped together into a halo (or perhaps a filament) in analogy with collapse to a point in the evolution of a spherical tophat overdensity.

The development of the algorithm and the PINOCCHIO code involves a great deal of detail and is well-beyond the scope of these lectures. However, this development is well-documented and the references above provide a good starting point for understanding the calculation.

9 A Minimal Reading List

The basic logic of the excursion set approach to halo formation and the construction of merger trees can be reconstructed by reviewing the following, *minimal* reading list.

- Bardeen et al. 1986
- Bond et al. 1991
- Lacey & Cole 1993
- Lacey & Cole 1994

- Sheth & Lemson 1999
- Somerville & Kolatt 1999

The various articles contained in the collection edited by Wax (1954) are an extremely valuable resource for understanding stochastic processes and deriving many of the basic results of excursion set theory. Of the articles reprinted in this collection, those by Chandrasekhar (1943), and Rice (1944, 1945) are probably of the most immediate interest.

Acknowledgments

I would like to thank Jeremy Tinker for making his numerical data available to me for these notes. This work was funded by the Kavli Institute for Cosmological Physics at the University of Chicago and by the National Science Foundation under grant NSF PHY 0114422.

References

- Bardeen, J. M., Bond, J. R., Kaiser, N., & Szalay, A. S. 1986, *ApJ*, 304, 15
- Bildhauer, S., Buchert, T., & Kasai, M. 1992, *A & A*, 263, 23
- Bond, J. R., Cole, S., Efstathiou, G., & Kaiser, N. 1991, *ApJ*, 379, 440
- Bond, J. R. & Myers, S. T. 1996, *ApJS*, 103, 1
- Bower, R. J. 1991, *MNRAS*, 248, 332
- Carroll, S. M., Press, W. H., & Turner, E. L. 1992, *ARAA*, 30, 499
- Chandrasekhar, S. 1943, *RMP*, 15, 2
- Cole, S. 1991, *ApJ*, 367, 45
- Cole, S. & Kaiser, N. 1988, *MNRAS*, 233, 637
- . 1989, *MNRAS*, 237, 1127
- Efstathiou, G., Frenk, C. S., White, S. D. M., & Davis, M. 1988, *MNRAS*, 235, 715

Epstein, R. A. 1983, MNRAS, 205, 207

Gao, L., Springel, V., & White, S. D. M. 2005, MNRAS, 363, L66

Gelb, J. M. & Bertschinger, E. 1994, ApJ, 436, 467

Jenkins, A., Frenk, C. S., White, S. D. M., Colberg, J. M., Cole, S., Evrard, A. E., Couchman, H. M. P., & Yoshida, N. 2001, MNRAS, 321, 372

Jing, Y. P. 1998, ApJL, 503, L9+

Kaiser, N. 1984, ApJL, 284, L9

Lacey, C. & Cole, S. 1993, MNRAS, 262, 627

—. 1994, MNRAS, 271, 676

Mo, H. J. & White, S. D. M. 1996, MNRAS, 282, 347

Monaco, P., Theuns, T., & Taffoni, G. 2002a, MNRAS, 331, 587

Monaco, P., Theuns, T., Taffoni, G., Governato, F., Quinn, T., & Stadel, J. 2002b, MNRAS, 564, 8

Peacock, J. A. & Heavens, A. F. 1990, MNRAS, 243, 133

Press, W. H. & Schechter, P. 1974, ApJ, 187, 425

Rice, S. O. 1944, Bell Systems Tech. J., Volume 23, p. 282-332, 23, 282

—. 1945, Bell Systems Tech. J., Volume 24, p. 46-156, 24, 46

Seljak, U. & Warren, M. S. 2004, MNRAS, 355, 129

Sheth, R. K. 1996, MNRAS, 281, 1277

—. 1998, MNRAS, 300, 1057

Sheth, R. K. & Lemson, G. 1999, MNRAS, 305, 946

Sheth, R. K., Mo, H. J., & Tormen, G. 2001, MNRAS, 323, 1

Sheth, R. K. & Pitman, J. 1997, MNRAS, 289, 66

Sheth, R. K. & Tormen, G. 1999, MNRAS, 308, 119

- . 2002, MNRAS, 329, 61
- . 2004, MNRAS, 350, 1385
- Somerville, R. S. & Kolatt, T. S. 1999, MNRAS, 305, 1
- Taffoni, G., Monaco, P., & Theuns, T. 2002, MNRAS, 333, 623
- Tormen, G. 1998, MNRAS, 297, 648
- Wax, N. 1954, Selected Papers on Noise and Stochastic Processes (New York: Dover Publication, 1954, edited by Wax, Nelson)
- Wechsler, R. H., Zentner, A. R., Bullock, J. S., Kravtsov, A. V., & Allgood, B. 2006, ApJ, In Press (astro-ph/0512416)